Submission under Review, Please Do not Distribute

Signal Integrity in Inter- and Intra-Chip Multi-Channel Communication

Jun Chen and Lei He
Electrical Engineering Department,
University of California, Los Angeles, 90095

ABSTRACT

Multi-channel communication has been used for on-chip and in-package high-bandwidth interconnection. Here, the interconnect connects multiple transceivers that transmit signals with high frequency carriers at different frequency bands, and frequency-dependent SNR (signal to noise ratio) and signal distortion need to be modeled and optimized. The interconnect in multi-channel communication is a multi-port lossy transmission line. In this work, we derive a closed-form model for SNR in multi-band and multi-port transmission lines with branches, and propose efficient figures of merit (FOMs) to minimize the signal distortion. Experiments show that the SNR model is accurate compared to SPICE simulation and the signal distortion FOMs are effective. We further automatically synthesize coplanar waveguide for radio-frequency (RF) interconnects with capacitive couplers for multi-channel communication. We minimize the total interconnect area under constraints of SNR and signal distortion. Compared to the published manual designs, the synthesized solution can reduce up to 80% area. Furthermore, the optimized solutions vary greatly with respect to number of ports, frequency bands, topologies and terminations, and therefore automatic synthesis is needed. In addition, the proposed SNR model and signal distortion FOMs can be applied to optimizing periodical signal such as clock.

1. INTRODUCTION

With the traditional base-band interconnect approaches its physical limits on communication bandwidth, multi-channel multi-band communication has been proposed to obtain high bandwidth for inter- and intra-chip interconnections [1, 2]. Here the signals are transmitted by high-frequency carriers over different frequency bands, and each frequency band can be further shared by multiple code-division communication channels terminated by transceivers. Because of the analog nature of the carrier and transceivers, frequency-dependent signal to noise ratio (SNR) and signal distortion need to be carefully modeled and optimized.

With multiple transceivers, the interconnect is a multi-port transmission line, which can be analyzed by numerical or analytical methods. Numerical methods such as circuit simulation [3, 4, 5, 6] and model order reduction [7, 8] provide generic solution to the voltage response in time or frequency domain, but they are too time consuming to be used in automatic synthesis. Analytic methods are efficient and can be used in synthesis. However, existing analytic models such as [9, 10, 11, 12] focus on delay and noise in time domain (and for only two ports), and there exists no analytical model for frequency-dependent SNR and signal distortion in a multi-port transmission line.

In this paper, we first derive an accurate model with linear complexity for the frequency-domain voltage response in branched transmission lines and then develop closed-form formulas for the amplitude of the signal and the reflection noise at receivers. We thus obtain the frequency-dependent SNR for each receiver. The SNR model is accurate compared to SPICE simulations. We also propose figures of merit (FOMs) to minimize the signal distortion in both signal phase and amplitude. The proposed SNR model and distortion FOMs can be applied to any multi-band multi-port transmission lines carrying high frequency carriers. It can also be applied to periodical signaling such as digital clock for analysis and optimization of signal amplitude and reflection noise. As an example, we apply our models to synthesis of coplanar waveguide (CPW) for on-chip multi-channel radio-frequency (RF) communication under constraints of SNR and signal distortion. We minimize the area of the interconnects with either perfect or imperfect terminations. The synthesis results demonstrate up to 80% less chip area compared to the published manual designs [1]. We also successfully synthesize an interconnection with multiple branches, which offers better routability than an unbranched interconnect but is too complicate to design manually. All the designs have been verified with time-domain transient simulation, which further validates our models. The synthesized designs vary with respect to the topologies, number of ports, frequency bands and terminations, and therefore show the effectiveness and necessity of the automatic synthesis process.

The rest of the paper is organized as follows: In section 2 we present the model for SNR and the figures of merit of signal distortion for multi-port transmission lines. In section 3 we formulate and solve the automatic synthesis problem for CPW for RF interconnection. We conclude the paper in section 4.

2. MODELS FOR MULTI-PORT TRANSMISSION LINES

In this section, we develop the models for multi-port branched transmission line. We assume the signal is transmitted via a carrier signal at a fixed frequency and develop our models in frequency domain. To avoid ambiguity, in this work we define a frequency channel as a FDMA (frequency division multiple access) channel with a fixed carrier frequency, and a communication channel as a signal path from a transmitter to a receiver. Each communication channel has only

one transmitter and one receiver. Each frequency channel can only have one transmitter, but it may have multiple receivers, and therefore can include multiple communication channels. We first show an accurate model for port voltage response, and then we develop a closed-form model for SNR of branched transmission line structures. In addition, we propose metrics for signal distortion.

2.1 Background of Transmission Line

A transmission line can be described as,

$$\frac{\partial V}{\partial x} = -(R + j\omega L)I \quad (1)$$

$$\frac{\partial I}{\partial x} = -(G + j\omega C)V \quad (2)$$

Where, R, L, G and C are the unit length resistance, inductance, conductance and capacitance of the transmission line. G is usually very small and can be ignored. The characteristic impedance of the transmission line is,

$$Z_0 = \sqrt{\frac{R + j\omega L}{G + j\omega C}} \quad (3)$$

The general solution to (1) and (2) is

$$V = A\exp(-\gamma x) + B\exp(\gamma x) \quad (4)$$

$$I = A/Z_0\exp(-\gamma x) - B/Z_0\exp(\gamma x) \quad (5)$$

where A and B are determined by boundary conditions. In (4) and (5) the component of $\exp(-\gamma x)$ is the forward wave propagating in the positive direction of x axis, and the component $\exp(\gamma x)$ is the backward wave propagating in the negative direction of x axis. γ is the propagation constant of the transmission line and is defined as

$$\gamma = \sqrt{(R + j\omega L)(G + j\omega C)} \quad (6)$$

The propagated wave is reflected at the terminations of the line. Assuming the impedance of the termination is Z_t, and the amplitudes of forward and backward waves are A and B, then the reflection ratio is

$$\Gamma = \frac{B}{A} = \frac{Z_0 - Z_t}{Z_0 + Z_t} \quad (7)$$

Reflections constitute part of the noise interfering with the propagated signal.

2.2 Port Voltage Response

Multiple branches and ports connected to the transmission line introduce extra discontinuities and reflections. In Figure 1, we show the interconnect model with multiple transceivers and branches. We assume linear transmitter and receiver models, and model each of them uniformly with a lumped impedance and an AC voltage source, where the amplitude of the voltage source for a receiver is zero. The capacitive coupler is modeled as a lumped capacitor. Because the circuit is linear, according to superposition principle we can consider each frequency channel separately.

We consider three types of discontinuities of the transmission line structure: ports, branching points and terminations. The segment between adjacent discontinuities is a continuous segment of transmission line, where the general solution of (4) and (5) still holds. The current and voltage between adjacent discontinuities k and $k+1$ can be written

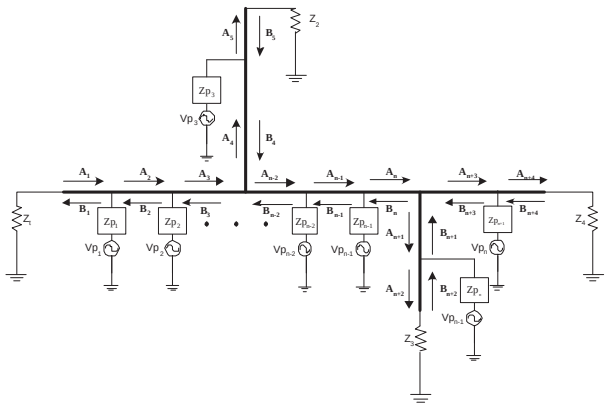

Figure 1: Circuit model of multi-port transmission line

as

$$V_k(x) = A_k\exp(-\gamma(x - x_k)) + B_k\exp(\gamma(x - x_{k+1})) \quad (8)$$

$$I_k(x) = \frac{A_k}{Z_0}\exp(-\gamma(x - x_k)) - \frac{B_k}{Z_0}\exp(\gamma(x - x_{k+1})) \quad (9)$$

where A_k and B_k are the amplitudes of the forward and backward waves (see Figure 1), Z_0 is the characteristic impedance of the transmission line and x_k is the location of discontinuity k. A_k and B_k are unknown variables to be determined by our voltage response model.

Each transmitter or receiver is a *port* to the interconnect. At a port k, by applying the KVL and KCL we have

$$V_k(x_k) = V_{k+1}(x_k) \quad (10)$$

$$Zp_k(I_k(x_k) - I_{k+1}(x_k)) = V_k(x_k) - Vp_k(x_k) \quad (11)$$

where Zp_k is the transceiver impedance and Vp_k is the transceiver voltage at port k.

At a branching point with n branches connected, we have incoming waves (A_i) and outgoing waves (B_i) on each connected branches, where $i = 1, 2, \ldots, n$. According to KCL,

$$\sum_{i=1}^{n}(A_i/Z_i - B_i/Z_i) = 0 \quad (12)$$

where Z_i is the characteristic impedance of branch i. Also because the branches are connected at the branching point, for any pair of branches i and j,

$$A_i + B_i = A_j + B_j \quad (13)$$

At the terminations of the transmission line, the voltage and current of the transmission line must satisfy the following equation

$$V = Z_t I \quad (14)$$

Assuming there are n ports and b branches, then there are $n + b$ segments of transmission lines and totally $2(n + b)$ unknown variables. (10)-(14) give $2n + 2b$ linear equations. Because only neighboring segments have coupling terms, the matrix is a sparse band matrix, the equation set can be efficiently solved by Gaussian elimination method with a time complexity of $O(n)$. We compare our voltage response model with SPICE simulations in Figure 2 for the voltage amplitude at different receivers. All SPICE simulations in this paper use a distributed RLC model with one RLC circuit for each wire segment of $5\mu m$. Other settings such as

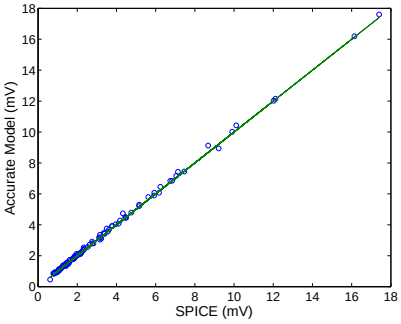

Figure 2: Voltage comparison between model in section 2.2 and SPICE simulation

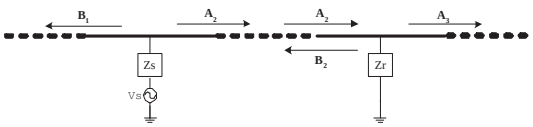

Figure 3: Simple model for transmitter and receiver port

transceiver impedances and locations are randomly generated. The number of ports is between 10 and 100, and we randomly choose the communication channel for comparison. According to the figure, our model almost perfectly matches the SPICE simulations.

2.3 SNR Model

To facilitate the computation of SNR and distortions, we develop models for signal and reflection noise amplitude at the receiver of one communication channel. Obviously each transmitter or receiver can only transmit signals on one frequency channel. Signals in other channels are filtered out by the receiver. Based on superposition principle, we can compute the waveform of each frequency channel separately. We assume the transceiver impedances are much larger than Z_0 so that the reflections from the ports are small and the transmission line is not disturbed much by the shunt impedances. With this assumption, we first derive a simplified model considering only the transmitter and the receiver in an unbranched transmission line without branches and ignoring other ports and terminations, and then extend the model to consider the effects of other ports, termination reflections and branching points.

2.3.1 Isolated Communication Channel

In this subsection, we consider one transmitter and one receiver on an unbranched transmission line without branches and ignore the effect of other ports and terminations. We also only consider first order effects on the signal at the receiver, which means we only consider the reflected wave from only one reflection, because waves after multiple reflections will have very small amplitudes. Under these assumptions, following the same notation as in section 2.2 and assuming the transmitter at port 1 and the receiver at port 2, the simplified model for the transmitter port and the receiver port are shown in Figure 3. According to (8)-(11), at the transmitter port we obtain

$$A_2 = \frac{Z_0/2}{Z_0/2 + Z_s} V_s \tag{15}$$

where Z_s and V_s are the impedance and voltage at transmitter port. B_2 is ignored at the transmitter port because we only consider the first order effect on the signal at the receiver. Similarly, at the receiver we have

$$A_3 = \frac{2A_2}{Z_0/Z_r + 2} \exp(-\gamma\ell) \tag{16}$$

$$B_2 = -\frac{A_2}{1 + 2Z_r/Z_0} \exp(-\gamma\ell) \tag{17}$$

where Z_r is the shunt impedance at the receiver port, and ℓ is the distance between the transmitter and the receiver. A_3 is the signal after the reflection at the receiver port. Since A_2 has been solved in (15), the voltage across receiver input resistance R_r is

$$V_r = \frac{R_r}{Z_r} A_3 = \frac{R_r Z_0/2}{(Z_0/2 + Z_r)(Z_0/2 + Z_s)} \exp(-\gamma\ell) V_s \tag{18}$$

which is the signal voltage at the receiver.

2.3.2 Effect of Multiple Ports

In this section, we further consider the effect of other ports and extend the model in section 2.3.1. When a propagating wave passes through a port, part of the signal is reflected according to (16) and (17). The situation is similar to that at a receiver in section 2.3.1. According to (16), the transmission rate for port k is

$$\xi_k = \frac{2}{Z_0/Zp_k + 2} \tag{19}$$

where Zp_k is the impedance of port k. According to (17), the reflection rate for port k is,

$$\rho_k = -\frac{1}{1 + 2Zp_k/Z_0} \tag{20}$$

Obviously, when Zp_k is large compared to Z_0, ξ_k is close to 1 and ρ_k is close to 0.

2.3.3 Effect of Terminations

According to (7), when the terminations are equal to the characteristic impedance Z_0, there will be no reflection from the terminations. Although the perfect termination may be designed, the terminations may be different from the ideal case because of the process variations. Imperfect terminations cause reflection and introduce extra noise. For terminations, we only concerns about the reflection noise. According to (7), the reflection coefficient of a termination with a lumped impedance of Z_t is,

$$\rho_t = \Gamma = \frac{Z_0 - Z_t}{Z_0 + Z_t} \tag{21}$$

2.3.4 Effect of Branch Junctions

In this section, we further extend our model to consider branched interconnections. A branched interconnection has *junctions* or *branching points* connecting two or more uniform interconnects. These junctions introduce extra discontinuity to the signal, and cause more loss of signal and reflection noise.

To consider the effects of junctions, we need to compute the signal transmission rate and reflection rate of each branch at the junction. Considering a junction connecting n branches, let the characteristic impedance of ith branch connected to the junction be Z_{0i}. For the a signal traveling on ith branch towards the junction, part of the signal will be reflected

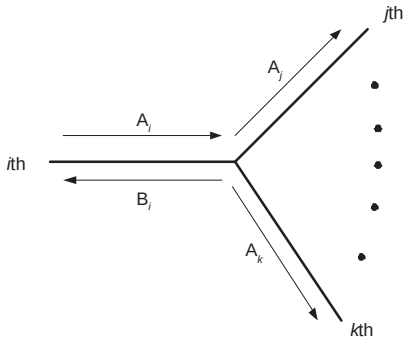

Figure 4: Circuit model of multi-port transmission line

due to the discontinuity and the rest will be transmitted to other branches. Since we will consider reflections from other discontinuity separately and temporarily ignore them, the signals on all the branches are shown in Figure 4. Using KCL and KVL, the reflection rate for branch i is derived as,

$$\rho_i = \frac{Z_{ti} - Z_{0i}}{Z_{ti} + Z_{0i}} \tag{22}$$

where,

$$Z_{t,i} = \frac{1}{\sum_{j \neq i} 1/Z_{0j}} \tag{23}$$

The transmission rate is,

$$\xi_i = \frac{2Z_{ti}}{Z_{ti} + Z_{0i}} \tag{24}$$

2.3.5 SNR

With the transmission and reflection rates of the discontinuities, including ports, junctions and terminations, the signal received by receiver r from transmitter s is derived as,

$$V_s = k_{s,r} \prod_{i \in s \to r, i \neq s} \exp(-l_{i-1,i}\gamma_{i-1,i})\xi_i \tag{25}$$

where $s \to r$ is the shortest path from s to r. $l_{i-1,i}$ is the branch length between $(i-1)$th discontinuity and ith discontinuity, $\gamma_{i-1,i}$ is the propagation constant of the branch, and ξ_i is the ith discontinuity's transmission rate. $k_{s,r}$ is a coefficient depending on the transmitter, and is defined as

$$k_{s,r} = \frac{R_r Z_{0r}/2V_s}{(Z_{0s}/2 + Z_s)(Z_{0r}/2 + Z_r)} \tag{26}$$

where R_r is the receiver input resistance, and Z_{0s} and Z_{0r} are the characteristic impedance of the branches where the transmitter and the receiver are located respectively.

Because we require small reflection rate for large SNR, higher order reflections result in negligible noise. Therefore, to compute the reflection noise from ports, we only consider the first order reflection. With all the discontinuities, the first order reflection noise at the receiver r from transmitter s is,

$$\begin{aligned} V_n &= k_{s,r} \sum_p \left(\prod_{i \in s \to p, i \neq s} \exp(-l_{i-1,i}\gamma_{i-1,i})\xi_i \cdot \rho_p \right. \\ &\quad \left. \cdot \prod_{j \in p \to r, j \neq s} \exp(-l_{j-1,j}\gamma_{j-1,j})\xi_j \right) \end{aligned} \tag{27}$$

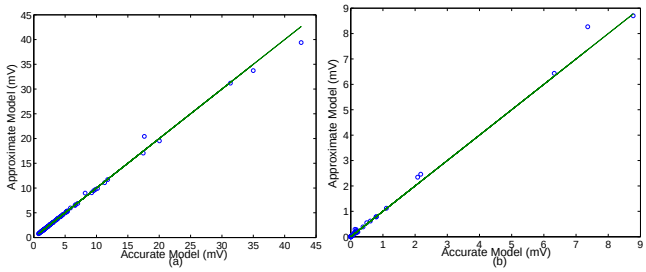

Figure 5: Comparison between numerical solution in section 2.2 and (a) formula (25) for signal at receivers; (b) formula (27) for reflection noise from ports

where discontinuity p is a discontinuity not on the shortest path from s to r, and ρ_p is the reflection rate of pth discontinuity.

(25) and (27) are verified by comparing with the results derived from the accurate model in section 2.2. The setting is randomly generated and the results are shown in Figure 5. From the figures, we can see the models are highly accurate compared to the numerical solution.

The signal at the receiver node is given in (25). The SNR at a receiver can be computed as,

$$\mathbf{SNR} = 10 \log \frac{\frac{V_s^2}{2R_r}}{\frac{V_n^2}{2R_r} + P_n} \tag{28}$$

where P_n is the power of the intrinsic receiver noise.

2.4 Metrics of Signal Distortion

The distortion of the waveform depends on attenuation and phase delay. The attenuation is defined as the reduction of the signal amplitude compared to the original signal. The phase delay is defined as

$$P(\omega) = -\frac{\Delta\phi(\omega)}{\omega} \tag{29}$$

where $\Delta\phi$ is the frequency dependent phase changing compared to the original signal and ω is the radial frequency of the carrier. A distortionless communication channel should have attenuation and phase delay, both uniform over the frequency band for a frequency channel.

To ensure small distortion we require limited difference of phase delay and attenuation in a frequency channel,

$$\Delta P = \frac{|P(\omega_0 - \omega_b) - P(\omega)|}{T_b} < 0.01 \tag{30}$$

$$\Delta M = \frac{|M(\omega_0 - \omega_b) - M(\omega_0)|}{M(\omega_0)} < 0.01 \tag{31}$$

where ω_0 is the carrier frequency, ω_b is the digital baseband frequency, and T_b is the baseband period. The phase P and amplitude M are computed according to (25). (30) and (31) are our FOM for signal distortion.

3. SYNTHESIS OF CPW

The SNR model and signal distortion FOM's proposed in section 2 can be applied to interconnection with high-frequency carriers and periodical signals such as clock. In this section, we apply these models to optimize the area of CPW-typed RF interconnection with multiple transceivers and multiple frequency bands.

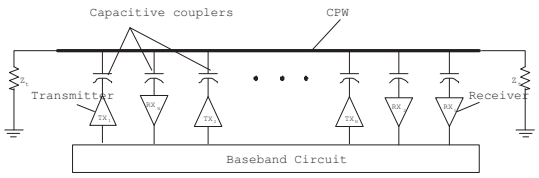

Figure 6: On-chip RF interconnection structure

3.1 Review of Multi-Channel Radio-Frequency Interconnects

Multi-channel multi-band interconnections have already been demonstrated on board and chip levels [13, 14], and recently for 3D integrated circuits [15]. The radio-frequency [1] interconnection is one of such type of interconnection. As shown in Figure 6 of an on-chip RF interconnect, the digital signal is first mixed with an RF carrier by a transmitter, and then coupled via a capacitive coupler into the interconnect, which is a transmission medium such as a coplanar waveguide (CPW) or a microstrip transmission line (MTL). The RF signal is transmitted bidirectionally along the interconnect, and picked up by multiple receivers via capacitive couplers and demodulated to obtain the original digital signal. Compared to the traditional interconnect, the RF interconnection has several advantages, such as low loss and distortion [1], immunity to digital switching noise [16] and less switching noise [16]. More importantly, a single RF interconnection can be simultaneously shared by several communication channels with multi-access techniques such as frequency-division (FDMA) and code-division (CDMA). By allocating frequency bands, FDMA allows multiple channels operated at different frequencies simultaneously access the interconnect without interfering with each other. CDMA further allows each frequency channel to be divided into subchannel by different encoding and real-time reconfiguration by changing the spreading codes.

The performance of an RF interconnection is limited by the bit-error rate (BER) at the receiver. To achieve the required BER, its signal to noise ratio (SNR) should be larger than a minimum bound [1], and the signal distortion should be controlled in certain range. Because the signal experiences loss and distortion through both the capacitive coupler and the interconnect, the size of the coupler and the geometries of RF interconnects must be designed properly for acceptable degree of loss and distortion.

3.2 Circuit Model of CPW

For CPW, we denote the signal wire width as w, the shielding wire width as g, and spacing between signal and shielding wires as s. The transmission line parameters can be computed from partial wire parameters as follows [12],

$$R = R_s + R_g/2 \quad (32)$$

$$L = L_s - 2L_{sg} + \frac{L_{gg}}{2} + \frac{L_g}{2} \quad (33)$$

$$C = 2C_{sg} + C_s \quad (34)$$

where R_s, C_s and L_s are the self resistance, ground capacitance and partial self inductance of the signal wire. R_g and L_g are the self resistance and partial inductance of the shielding wires. C_{sg} and L_{sg} are the coupling capacitance and partial mutual inductance between the signal wire and a shielding wire. L_{ss} is the partial mutual inductance between the two shielding wires. We extract frequency-dependent resistance and partial inductance with FastHenry [17] and calculate the capacitance by

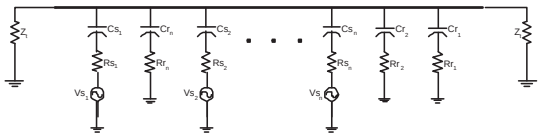

Figure 7: Circuit model of RF interconnect

$$C = \frac{1}{c^2 L} \quad (35)$$

where uniform dielectric is assumed and c is the speed of light in the dielectric. The capacitive couplers of transceivers are modeled by lumped capacitors, and the transceivers are modeled by linear drivers. The circuit model of the entire RF interconnection is shown in Figure 7.

3.3 Automatic Synthesis

We assume that the transceivers have been given and the noise characteristics of the receivers are determined beforehand. We minimize the area under the constraints of SNR and distortion by adjusting the geometries of the interconnection and the size of each capacitive coupler. SNR must be larger than a minimum value. For small distortion, we require the solutions satisfy FOM (30) and (31) for signal distortion. The problem is formulated as below,

FORMULATION 1. *Given the transceivers and the noise characteristics of receivers P_n (see (28)) , determine the signal wire width w, signal-shield spacing s, shielding width g, and the size of each capacitive coupler such that the total area of the interconnect and capacitive couplers is minimized under the constraint that at each receiver our FOM (30) and (31) for signal distortion are satisfied, and SNR is larger than the required minimum SNR.*

Our closed-form models in (28), (30) and (31) enable us to use simulated annealing (SA) algorithm to optimize the wire geometries and the size of each capacitive coupler in a relatively short run time. Also, because there are only a few RF interconnects in one chip, SA algorithm is affordable. The objective function is defined as

$$F(w_j, s_j, g_j, C_i) = K_a A + \sum_i (K_s FS_i + K_{pd} FP_i + K_{ad} FA_i) \quad (36)$$

Where K_a, K_s, K_{pd} and K_{ad} are weights, A is the total area of the RF interconnect and couplers. w_j, s_j and g_j are the signal wire width, signal to shield spacing and shield width of branch j, and C_i's are the sizes of capacitive couplers. We also require that the couplers totally overlap the central signal wire of CPW and do not overlap each other. We assume that the coupler can be implemented with a capacitance density of $0.5fF/\mu m^2$[14], then

$$A = \sum_{j=1}^{b} l_j (w_j + 2s_j + 2g_j) + \sum_{i=1}^{n} \frac{C_i}{0.5}$$

FS_i, FP_i and FA_i in (36) are the penalty functions for the violation of the constraints of SNR, phase delay and attenuation at receiver i respectively. For each receiver,

$$FS_i = \begin{cases} 0 & (SNR_i > \underline{SNR}) \\ \underline{SNR} - SNR_i & (SNR_i < \underline{SNR}) \end{cases}$$

Table 1: Comparison between manual design and automatic synthesis

design	w	s	g	total width	C_s	C_r
manual	-	-	-	$100\mu m$	100fF	100fF
synthesis	$2.2\mu m$	$6.0\mu m$	$1.1\mu m$	16.8 μm	51fF	49fF

where $\underline{SNR}$ is the minimum SNR.

$$FP_i = \begin{cases} 0 & (\Delta P_i < \overline{\Delta P_i}) \\ \Delta P_i - \overline{\Delta P_i} & (\Delta P_i > \overline{\Delta P_i}) \end{cases}$$

where ΔP_i is defined in (30) and $\overline{\Delta P}_i$ is the upper bound of phase delay difference. Similarly,

$$FA_i = \begin{cases} 0 & (\Delta M_i < \overline{\Delta M_i}) \\ \Delta M_i - \overline{\Delta M_i} & (\Delta M_i > \overline{\Delta M_i}) \end{cases}$$

where ΔM_i is defined in (31) and $\overline{\Delta M}_i$ is an upper bound FOM of attenuation difference.

There are four types of moves in our simulated annealing scheme: (1) changing w_j; (2) changing g_j; (3) changing s_j; (4) changing C_i. Branch i and coupler j are randomly picked. During the process, we always make sure that the coupler fully overlapped with the transmission line. In each movement, we randomly increase or decrease the chosen geometric parameter by a factor from 0% to 5%. We start the SA with initial temperature of 20 and terminate it at 0.001. The temperature is decreased by a factor of 0.95 and the number of moves at a particular temperature is 300.

3.4 Experiment Results

3.4.1 Perfect Terminations

We first assume that the interconnection is unbranched and the terminations are perfect and therefore there is no reflection from the terminations. For comparison we first synthesize an RF interconnect with the same specifications as in [1]. The interconnect length is $1cm$, the carrier frequency is 5GHz, the baseband frequency is 275MHz, the transceiver impedance is 2kΩ, the transmitter voltage is 1.8V and the power of receiver intrinsic noise is -67dBm. The minimum SNR is set to 20dB. One transmitter and one receiver are at the opposite ends of the interconnect. As shown in Table 1 the synthesis result reduces the total interconnect width including spacing by 80% and the coupler size by 50% compared to manual design in [1]. To verify our design, we carry out transient simulation with SPICE. Linear transceivers are assumed in the simulation. The input digital signal pattern is alternative "0" and "1". Figure 8 plots input and output waveforms with clear repeated "01" pattern. The signal amplitude is $14mV$ and therefore the SNR is 21dB which satisfies the lower bound constraint of 20dB.

We also carried out synthesis with different transceiver impedance and various numbers of FDMA channels and transceivers. The FDMA channels are allocated from 10 to 110 GHz with 20GHz for each channel. When there is only one FDMA channel, 10-30GHz channel is used. The digital baseband frequency is 1GHz. The transmitter voltage amplitude, the receiver amplifier noise and the minimum SNR are the same as those in the experiment presented above. The transmitters and receivers have the same impedance and uniformly distributed along the interconnect. Table 2 summarizes some sample results. In this table, we report the average capacitive coupler size for transmitters and receivers respectively. From the results, it is clear that the synthesized solution for different input parameters varies greatly. The total area can be 3× different. Generally, larger transceiver impedance, longer communication distance and more ports lead to wider interconnect and larger area. Note the manual design assumes uniform capacitive coupler size for all ports, but we find that the coupler size can vary a lot depending on the channel, location and type of each port. The difference can be up to 20× in the same design case. More interestingly, when there are multiple ports, the capacitive couplers for receivers are much smaller than those for transmitters, which helps reduce reflection and increase the signal transmission rate.

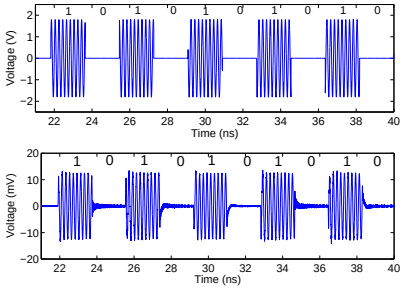

Figure 8: Transient waveform. (a) upper: Input; (b) lower: Output

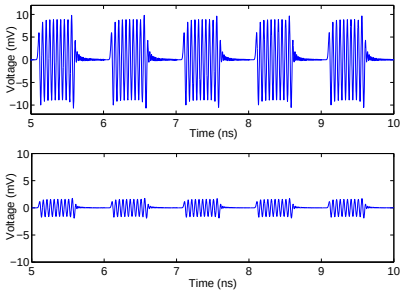

Figure 9: Transient waveforms of interconnect configuration case 4 in Table 2. (a) upper: with matched interconnect; (b) lower: with mismatched interconnect synthesized for case 1.

To show the effectiveness of the synthesis, we also carried out transient simulations with different interconnect settings. In Figure 9, (a) shows the waveform at port 40 of the case 4 in Table 2 with the matched interconnect from synthesis and (b) shows the waveform with mismatched interconnect synthesized for case 1. It is clear that (a) satisfies the SNR constraints while (b) has only 2mV signal amplitude and SNR of 7dB, which is far blow the required bound.

3.4.2 Imperfect Terminations

In reality, the terminations are often mismatched due to process variations. In this section, we study the impact of imperfect terminations on the synthesis results. The RF interconnection under study is 1cm long with 5 channels allocated from 10 to 110 GHz with 20GHz for each channel. Each channel has 1 transmitter and 4 receivers. The locations of the ports are randomly selected. The lower bound of SNR is set to 15dB. We define the mismatch degree as the relative difference between the real termination and the perfect termination. Figure 10 shows the trend of the interconnect area and coupler size with the increasing of different degrees of mismatch. It is clear the total interconnect area

Table 2: Automatic synthesis results. All results meet SNR and distortion requirements.

	system specifications				synthesis result					
case	ports	channels	$Rp(\Omega)$	$l(cm)$	$w(\mu m)$	$s(\mu m)$	$g(\mu m)$	Area(μm^2)	Avg. $C_s(fF)$	Avg. $C_r(fF)$
1	2	1	500	1	1.6	0.8	1.2	56360	88	92
2	2	1	1000	1	1.8	2.3	1.1	85916	95	98
3	2	1	1000	3	4.3	3.5	3.0	517773	108	113
4	40	5	1000	1	4.5	4.5	3.0	196305	40	19

increases with the increasing of mismatch. Initially the area increases slowly and the mismatch has the less effects on the synthesis results when the mismatch is less than 10%. However, when the mismatch gets close to 15%, the area increases dramatically to about 3 times of the area of perfect matching case. The coupler size has the similar trends but with much smaller slope. According to the previous discussion in subsection 2.3.3, the SNR with only the reflection noise from the terminations decreases to 16dB when the mismatch is 15%. When the mismatch is larger than 15%, no valid solutions are found.

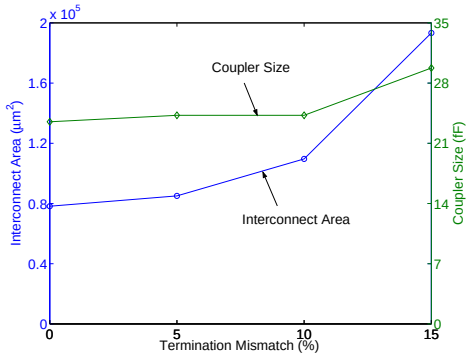

Figure 10: Interconnect area and coupler size with different termination mismatch. The solutions meet the SNR and distortion requirements.

3.4.3 *Branched Interconnection*

In the subsections above we present experiment results for unbranched interconnections. Below, we synthesize an RF interconnection with branches. In this experiment, the impedances of all the transceivers are 1000Ω and we assume perfect terminations. The minimum SNR is set to 15dB. The transmitter input voltage is 1.8v. In Figure 11 we show one example of branched RF interconnects. The structure has one main interconnect branch and three sub branches.

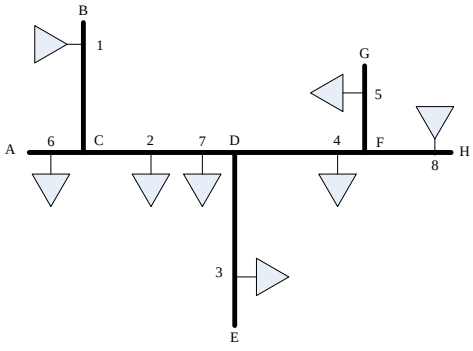

Figure 11: A sample structure of branched RF interconnects.

Table 3: Geometries of each CPW segment.

branch	length(μm)	w(μm)	s(μm)	g(μm)	area (μm^2)
AC	1000	0.5	5.1	0.1	10900
BC	5000	2.7	6.1	1.5	89500
CD	5000	5.8	2.3	2.3	75000
DE	6000	1.8	6.1	0.9	94800
DF	4000	6.4	3.4	2.2	70400
FG	3000	0.8	8.0	0.3	52200
FH	2000	2.3	10	1.1	90400

Table 4: Coupler and signal amplitude for ports

Port	1	2	3	4	5	6	7	8
Coupler (fF)	67	13	47	32	58	12	21	48
SPICE (mV)	-	14.8	8.9	9.9	8.7	14.5	9.0	-
Model (mV)	-	14.6	8.7	10.3	8.2	13.4	8.7	-
Error (%)	-	-1.3	-2.2	4.0	-5.7	-7.6	-3.3	-

However, since there is already discontinuity at branching points, we allow each segment between branching points in the main branch have different geometries to further optimize the structure. Therefore, segment AC, CD, DF and FH can have different optimal geometries. All these branches are CPW. There are two channels and each of them has one transmitter. Channel 1 is at frequency of 10GHz and has four receivers at port 2, 3, 4 and 5 receiving signal from the transmitter at port 1. Channel 2 is at frequency of 20GHz and has two receivers at port 6 and 7 receiving signal from the transmitter at port 8. Table 3 shows the synthesized geometries of each segment and table 4 shows the synthesized value of the coupling capacitor at each port. From the results we can see the synthesized values for each segments are different. For segments shared by signal paths such as CD and DF, signal wire width and shield width are large to reduce the attenuation of the signal. Sub-branch segments have smaller signal width and shield width, but the spacing between them can be large to match the impedance at the branching points. For each channel, the transmitter has the largest coupling capacitor compared to receivers, and receivers farther from the transmitters has larger coupling capacitors than those closer to the transmitters.

We further carry out SPICE simulation to verify the results. The amplitudes of signal at each receiver from both SPICE simulation and the proposed model are shown in table 4. We can see the results of our model closely match those from SPICE simulation. In Figure 12, we show the waveforms at transmitter 1 and receivers 2 and 5 from SPICE simulation. Port 5 is farthest from port 1 and its signal amplitude is just enough to meet 15dB minimum requirement. The signal amplitude at port 2 is slightly larger because it is closer to the transmitter.

4. CONCLUSION AND DISCUSSIONS

Multi-channel communication with multiple transceivers can be modeled as multi-port lossy transmission lines. To efficiently analyze and design such interconnection, we first developed an efficient model with linear complexity to compute the voltages of multi-port transmission line, and then derived closed-form models for the amplitudes of signal and

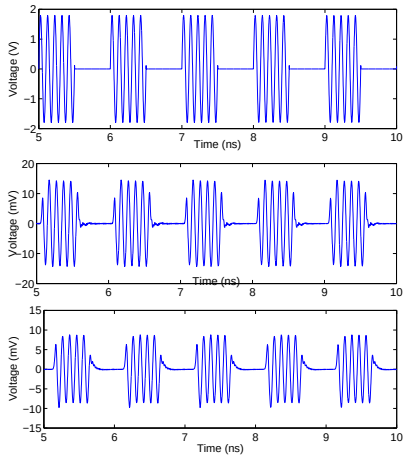

Figure 12: Transient waveforms at various ports. (a)upper: Port 1 (transmitter); (b)middle: Port 2; (c)lower: Port 5

reflection noise to efficiently compute the SNR. We also proposed figures of merit to minimize the distortion in signal phase and amplitude. Experiments show that the SNR model is accurate compared to SPICE simulation and signal distortion FOMs are effective. The proposed SNR model and distortion FOMs can be applied to any multi-band multi-port transmission lines using high frequency carriers, and to periodical signaling such as clock. We applied our models to automatic synthesis of the CPW geometries and capacitive couplers for branched multi-channel multi-port RF interconnection. We minimized the total interconnect area under the constraints of SNR and signal distortion. The solutions are verified with time-domain transient simulations. Compared to the published manual designs, the synthesized solutions can save up to 80% chip area. The complexity and large difference in the various optimized solutions demonstrate the necessity and effectiveness of the automatic synthesis process. For future work, we plan to extend our models to further consider active devices and apply these models to other communication interconnection schemes and clock design.

5. REFERENCES

[1] M. F. Chang, V. P. Roychowdhury, L. Zhang, H. Shin, and Y. Qian, "RF/wireless interconnect for inter- and intra-chip communications," *Proceedings of the IEEE*, vol. 89, pp. 456–466, 2001.

[2] Q. Gu, Z. Xu, J. Kim, J. Ko, and M. F. Chang, "Inter and intra-chip clock signal distribution using microwaves," in *Proc. IEEE Int. Workshop Clock Distribution Network*, 1997.

[3] F. Y. Chang, "Waveform relaxation analysis of rlcg transmission lines," *IEEE Trans. on Circuits and Systems*, pp. 1394–1415, Nov 1990.

[4] J. Roychowdhury, A. R. Newton, and D. O. Pederson, "An impulse-response based linear time-complexity algorithm for lossy interconnect simulation," in *Proc. Int. Conf. on Computer Aided Design*, 1991.

[5] S. Lin and E. S. Kuh, "Transient simulation of lossy interconnects based on the recursive convolution formulation," *IEEE Trans. on Circuits and Systems I: Fundamental Theory and Applications*, vol. 39, pp. 879–892, 1992.

[6] M. J. Gander and A. E. Ruehli, "Solution of large transmission line type circuits using a new optimized waveform relaxation partitioning," in *IEEE International Symposium on Electromagnetic Compatibility*, 2003.

[7] T. K. Tang, M. S. Nakhla, and R. Griffith, "Analysis of lossy multiconductor transmission lines using the asymptotic waveform evaluation technique," *IEEE Trans. Microwave Theory Techiques*, vol. 39, pp. 2107–2116, 1991.

[8] A. Odabasioglu, C. M, and L. Pileggi, "PRIMA: Passive reduced-order interconnect macromodeling algorithm," *IEEE Trans. on Computer-Aided Design of Integrated Circuits and Systems*, 1998.

[9] A. Kahng and S. Muddu, "An analytical delay model for RLC interconnects," in *Proc. IEEE Int. Symp. on Circuits and Systems*, 1996.

[10] Y. Gao and D. F. Wong, "Shaping a VLSI wire to minimize delay using transmission line mode," in *Proc. Int. Conf. on Computer Aided Design*, 1998.

[11] J. A. Davis and J. D. Meindl, "Compact distributed RLC interconnect models. I. single line transient, time delay, and overshoot expressions," *IEEE Transactions on Electron Devices*, pp. 2068 –2077, November 2000.

[12] R. Escovar and R. Suaya, "Transmission line design of clock trees," in *Proc. Int. Conf. on Computer Aided Design*, 2002.

[13] W. Ryu, A. Wai, F. Wei, W. L. Lai, and J. Kim, "Over ghz low-power RF clock distribution for a multiprocessor digital system," *IEEE Transactions on Advanced Packaging*, vol. 25, pp. 18–27, 2002.

[14] H. Shin and M. F. Chang, "1.1 Gbit/s RF-interconnect based on 10 GHz RF-modulation in 0.18 m CMOS," *Electronics Letters*, vol. 38, pp. 71–72, 2002.

[15] Q. Gu, Z. Xu, J. Kim, J. Ko, and M. F. Chang, "Three-dimensional circuit integration based on self-synchronized RF-interconnect using capacitive coupling," in *Symposium on VLSI Technology*, 2004.

[16] H. Shin, Z. Xu, K. Miyashiro, and M. F. Chang, "Estimation of signal-to-noise ratio improvement in RF-interconnect," *Electronics Letters*, vol. 38, pp. 1666–1667, 2002.

[17] M. Kamon, M. Tsuk, and J. White, "Fasthenry: a multipole-accelerated 3d inductance extraction program," *IEEE Trans. on MIT*, 1994.